Different Local Structures of Mo and Nb Polyhedra in the Oxide-Ion-Conducting Hexagonal Perovskite-Related Oxide $Ba_3MoNbO_{8.5}$ Revealed by ^{95}Mo and ^{93}Nb NMR Measurements

Masataka Tansho,[*,†] *Atsushi Goto,*[†] *Shinobu Ohki,*[†] *Yuuki Mogami,*[†] *Yuichi Sakuda,*[‡] *Yuta Yasui,*[‡] *Taito Murakami,*[‡▽] *Kotaro Fujii,*[‡] *Takahiro Iijima,*[§] *and Masatomo Yashima*[‡]

[†]NMR Station, National Institute for Materials Science (NIMS), 3-13 Sakura, Tsukuba 305-0003, Japan

[‡]Department of Chemistry, School of Science, Tokyo Institute of Technology, 2-12-1-W4-17, O-okayama, Meguro-ku, Tokyo, 152-8551, Japan

[§]Institute of Arts and Sciences, Yamagata University, Yamagata 990-8560, Japan

ABSTRACT

The oxide-ion conductor $Ba_3MoNbO_{8.5}$, the oxide-ion and proton conductor $Ba_7Nb_4MoO_{20}$, and their hexagonal perovskite-related oxides are important groups of materials because of their high ionic conductivity. The structure of the ion-conducting layer of these materials has not been clarified because of their complex structure and the difficulty in distinguishing between Mo and Nb. In this study, we separately detected ^{95}Mo and ^{93}Nb by solid-state nuclear magnetic resonance (NMR) measurements to directly observe the Mo/Nb coordination in the high oxide-ion conductor $Ba_3MoNbO_{8.5}$. The results showed that the number of revealed peaks was different for ^{93}Nb and ^{95}Mo. For the two chemical shifts from ^{93}Nb NMR, the more intense peak was attributed to a NbO_6 octahedron in the conducting layer, while the less intense peak was ascribed to a NbO_4 tetrahedron in the conducting layer or a NbO_6 octahedron in the non-conducting layer. Four peaks were observed in the ^{95}Mo NMR of the ^{95}Mo-enriched sample. One peak was attributed to the MoO_6 octahedron in the non-conducting layer. The other three peaks attributed to the conducting layer were only interpreted by assigning either one or two of them to the MoO_5 polyhedra, which are speculated to play an important role in ionic conduction. Presumably, these are the first results supporting the presence of MoO_5 in the ion-conducting layer of oxide-ion conductors, and Mo likely plays an important role in ionic conduction. The analysis of the local structure of Mo and Nb oxide polyhedra by NMR is an important tool for understanding the nature of ionic conduction because it provides element-independent information. It is therefore expected to contribute to the further development of oxide-ion conductors.

INTRODUCTION

The development of solid oxide-ion (O^{2-}) conductors has led to a range of energy and environmental technologies, including gas sensors, solid oxide fuel cells (SOFCs), and oxygen separation membranes. Research on the high energy efficiency of SOFCs at low temperatures has led to the discovery of new oxide-ion conductors and an improved understanding of the diffusion mechanisms of oxide ions.[1–5] Recently, it has been reported that hexagonal perovskite-based materials such as $Ba_3MoNbO_{8.5}$ and the related materials,[6–17] which are oxide-ion conductors, as well as $Ba_7Nb_4MoO_{20}$[18,19] and $Ba_7Ta_{3.7}Mo_{1.3}O_{20.15}$,[20] which are mixed conductors of oxide ions and protons, show high ion conductivity. For example, $Ba_3MoNbO_{8.5}$ exhibits oxide-ion conduction over a pO_2 range of 10^{-20}–1 atm with a bulk conductivity of 2.2×10^{-3} Scm^{-1} at 600 °C. The complex structures of these materials have been shown to be related to their high ionic conductivity. In $Ba_7Ta_{3.7}Mo_{1.3}O_{20.15}$, the structural analysis of synchrotron X-ray diffraction data with the support of density functional theory calculations shows that Mo^{6+} is preferentially present in the conduction layer.[20]

For $Ba_3MoNbO_{8.5,}$ represented by $A_3B_2O_{8.5}$ (A = Ba, B = M = Mo/Nb), the structure is based on the 9R polytype $A_3B_3O_9$ and a cation-anion deficient derivative of palmierite $A_3B_2O_8$.[6] Although it was initially believed that one-third of the vacancies were distributed in the B-site,[7] it has recently been demonstrated that up to two cations can occupy each M1–M2–M1 polyhedral stack, and that the M2-site is distributed in two equivalent positions along the *c*-axis, maintaining the $M2O_6$ octahedral structure (Figure 1).[14] Here, the O2 and O3 oxygen atoms coordinated to M1 are statistically distributed with an occupancy of less than 1, whereas the O1 oxygen atom coordinated to M2 is coordinated with an occupancy of 1.[7,14] In addition, the M1 sites were initially believed to contain only $M1O_4$ and $M1O_6$ polyhedra, and the oxide-ion conductivity was correlated with the change in the ratio of $M1O_4$ tetrahedra to $M1O_6$ octahedra with increasing temperature using

Rietveld refinement.[8,10] However, the very large atomic displacement parameter of O2 obtained from single-crystal diffraction results suggests that five-fold coordination is also very likely (Table 1).[14,17] Oxide ions were also found to migrate two-dimensionally through the mixed oxygen sites of O2 octahedra and O3 tetrahedra on the O2–O2–O2 faces of the $M1O_{5-\varepsilon}$ polyhedra, where ε is the oxygen vacancy concentration.[15] The O2/O3 disordering makes the minimum neutron scattering length densities on the O2−O3 path higher, which enhances oxide-ion conductivity, leading to higher activation energies of $Ba_3WNbO_{8.5}$ compared with $Ba_3MoNbO_{8.5}$.[12] Recently, modeling using a combination of Bragg, $D(r)$, and $F(q)$ data from neutron scattering experiments suggested a preference for $M1O_5$ polyhedra in $Ba_3MoNbO_{8.5}$.[16] In this study, the coordination numbers of the M cations were determined using a cut-off length based on the M–O distance histograms obtained from reverse Monte-Carlo simulations. The variable coordination environment and coordination dynamics of the M1 site in $Ba_3MoNbO_{8.5}$ are believed to be important for creating a low-energy transfer pathway for oxide ions; however, these structures are usually studied by X-ray diffraction, neutron scattering, and electron diffraction, assuming an even distribution of Mo and Nb at each site and analyzed as if there were averaged Mo and Nb atoms, although there were no averaged Mo/Nb atoms.[6–17] This is because X-rays, neutrons, and electrons all have a close scattering ability, rendering distinguishing between Nb and Mo difficult. In addition, the reverse Monte-Carlo simulation is very model-dependent. Hence, more reliable and direct evidence of the presence of $M1O_5$ polyhedra in $Ba_3MoNbO_{8.5}$ is necessary.

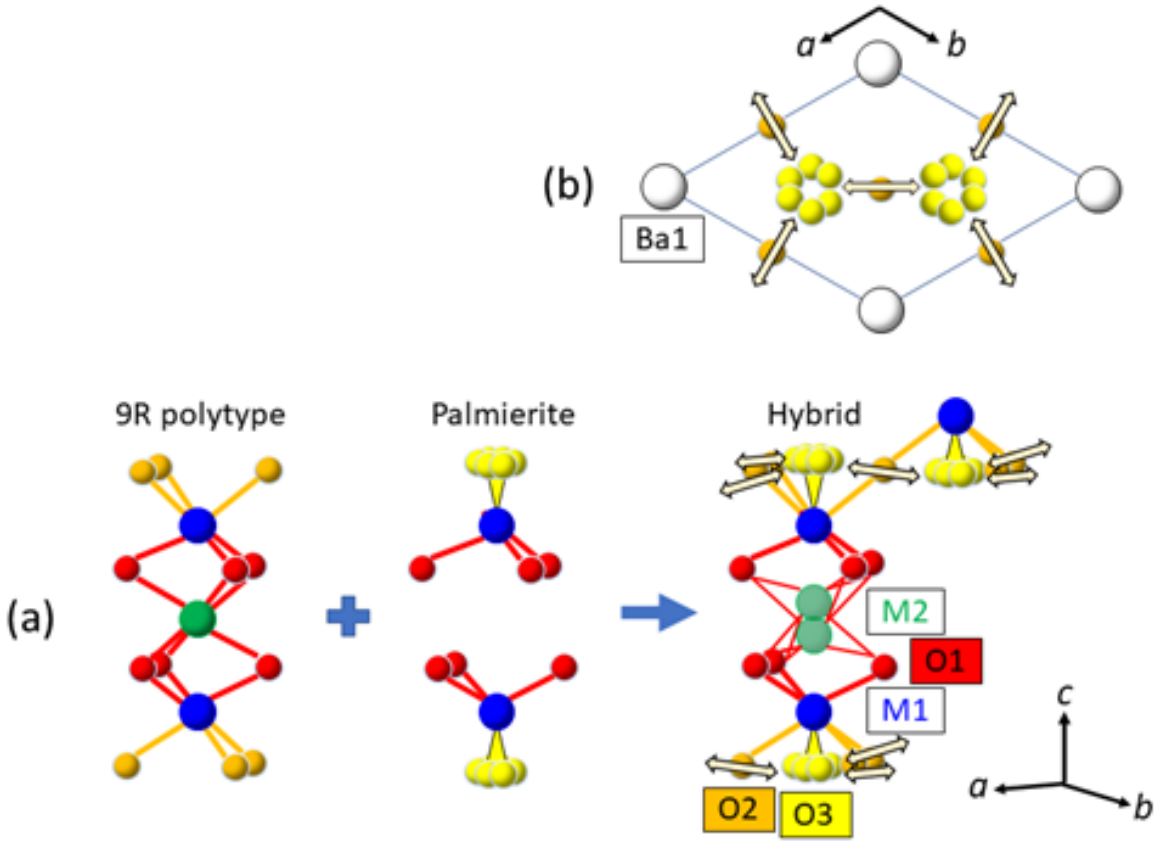

Figure 1. Part of the crystal structure of $Ba_3MoNbO_{8.5}$. (a) Averaged structure is represented as a hybrid consisting of the overlapping 9R polytype and palmierite subunits, where M is Mo/Nb, the space group is $R\bar{3}m$, and M2 sites are C_3 symmetric and distributed in two positions along the *c*-axis. The occupancies of M1 and M2 at room temperature are 0.881 and 0.119, respectively.[14] (b) Structural cross-sectional in the *c*-axis direction. The layer containing partially occupied O2/O3 sites is shown. The arrows in both directions indicate the diffusion directions of oxide ions. In the M1 site, in addition to $M1O_4$ and $M1O_6$, the $M1O_5$ polyhedron is likely an important structure related to oxygen diffusion in the pathway via O2 and O3. Each site is described in the same way as in ref 7.

Table 1. Local structures known and suggested to exist in $Ba_3MoNbO_{8.5}$

site [a]	Local structure known to exist	Local structure suggested to exist
M1	$M1O1_3O3_1$ and $M1O1_3O2_3$	$M1O_5$
M2	$M2O1_6$	–

[a]Both M1 and M2 are for (Nb/Mo) sites, and the notation is the same as in ref. 7.

Nuclear magnetic resonance (NMR), which, in principle, directly reflects the electronic state around the nucleus, is advantageous for determining local structures. Specifically, we measured the solid-state NMR of ^{95}Mo and ^{93}Nb in $Ba_3MoNbO_{8.5}$ for two reasons: the ease of distinguishing between Mo and Nb, and the possibility of splitting the signal for each coordination number, which would include the MO_5 polyhedron.[21–26] For the measurement of Mo, ^{95}Mo was selected from NMR-active nuclei because of its suitability for high-resolution analysis; NMR measurements were also conducted on a sample enriched with ^{95}Mo to improve sensitivity. These NMR measurements revealed the diffusion mechanism of oxide ions by analyzing the individual coordination structures of Nb and Mo, providing new opportunities for the design of oxide-ion conductors with hexagonal perovskite-related structures.

EXPERIMENTAL SECTION

$Ba_3MoNbO_{8.5}$ and ^{95}Mo-enriched samples were synthesized using a solid-state reaction method. The starting materials were high-purity (>99.9%) powders of $BaCO_3$, MoO_3, and Nb_2O_5 for $Ba_3MoNbO_{8.5}$ and high-purity (>99.9%) powders of $BaCO_3$; $^{95}MoO_3$ (^{95}Mo = 95.5 atom% of Mo isotopes, Trace Sciences International); and Nb_2O_5 for ^{95}Mo-enriched samples. The

$Ba_3MoNbO_{8.5}$ sample was synthesized as previously reported.[15] The ^{95}Mo-enriched sample was synthesized as follows: the starting materials were weighed in a molar ratio of Ba:Mo:Nb = 3:1:1 and then mixed and ground for approximately 1 h in an agate mortar as dried powders and as ethanol slurries. This mixture was calcined in air at 900 °C for 12 h. The calcined sample was ground for approximately 1 h in an agate mortar. Thereafter, the mixture was uniaxially pressed into pellets at approximately 250 MPa and sintered in air at 1100 °C for approximately 48 h. The calcined pellets were crushed in a WC mortar and ground for approximately 1 h in an agate mortar.

All NMR measurements were conducted with a fabricated 3.2-mm single resonance magic angle spinning (MAS) probe at 18.79 T without temperature control, where the resonance frequencies for ^{95}Mo and ^{93}Nb were 52.16 and 195.84 MHz, respectively. The natural abundances and spin number, *I*, were 15.7% and 5/2 for ^{95}Mo and 100% and 9/2 for ^{93}Nb. All samples were rotated at 20 kHz. A 0 ppm 2.0 M Na_2MoO_4 solution was used as a reference for the chemical shifts of ^{95}Mo, and −1093 ppm[22,27] at 18.79 T in $NaNbO_3$ (Sanwa Chemical Industry, 99.9%) was used as a convenient secondary chemical shift reference for the chemical shifts of ^{93}Nb instead of a saturated solution of $NbCl_5$ in acetonitrile at 0 ppm. A JEOL ECA 800 NMR spectrometer was used for the one-dimensional measurement of ^{95}Mo and two-dimensional measurement of ^{93}Nb. A JEOL ECZR 800 NMR spectrometer was used for the one-dimensional measurement of ^{93}Nb. One-dimensional ^{95}Mo spectra were acquired with 13,000–22,000 scans using either a single pulse of 1.2–1.6 μs, corresponding to a liquid standard π/6 pulse, or a spin-echo sequence[28] (2.5 and 5.0 μs) with a relaxation delay of 20 s. Due to the severe baseline distortion in single-pulse ^{93}Nb MAS measurements, one-dimensional ^{93}Nb spectra were acquired in a spin-echo sequence[28] (2.0 and 4.0 μs) with 1,024 scans, and the

relaxation delay was set to 1 s. Here, 2.0 μs corresponds to the π/3 pulse of solid $NaNbO_3$. For the multi-quantum (MQ) MAS NMR measurement of ^{93}Nb, we employed three-quantum (3Q) MASNMR, a type of MQMAS NMR, measurement with a three-pulse (2.0, 0.9, and 15 μs) sequence using a zero-quantum filter, as proposed by Amoureux et al.[29] Here, the spectrum was recorded with 264 transients averaged for each of the 1024 $t1$ points and a relaxation delay of 0.2 s, which was sufficient to obtain an adequate signal-to-noise ratio.

The magnitude of the quadrupole coupling constant, C_Q, of the ^{95}Mo resonance for ^{95}Mo-enriched $Ba_3MoNbO_{8.5}$ was evaluated using the DMFIT simulation software package.[30] In the case of quadrupole nuclei such as ^{93}Nb, the apparent shift measured by one-dimensional MAS NMR, δ_{MAS}, is usually different from the isotropic shifts, δ_{iso}. For solid solutions such as $Ba_3MoNbO_{8.5}$, it is difficult to separate the contribution of asymmetric parameters from the P_Q values because the line widths are broadened by the distribution of chemical shifts,[31] and the analysis of the 3QMAS result was performed as follows:[32–35] the positions of the experimental resonances (δ_{F1} and δ_{F2}) in the F1 and F2 dimensions of the sheared MQMAS spectrum and quadrupole product, P_Q, (the same as the second-order quadrupolar effect (SOQE)) are calculated as

$$\delta_{iso} = \frac{17\delta_{F1} + 10\delta_{F2}}{27} \quad (1)$$

and

$$P_Q = \left(\frac{10}{27} \cdot \frac{17}{3}\right)^{1/2} \frac{[4I(2I-1)]}{[4I(I+1)-3]^{1/2}} \nu_L \cdot 10^{-3} (\delta_{F1} - \delta_{F2})^{\frac{1}{2}}. \quad (2)$$

Here, δ_{F1} and δ_{F2} are chemical shifts in the triple and single quantum dimensions, respectively, and ν_L is the Larmor frequency. P_Q is related to C_Q by $P_Q = C_Q (1 + \eta^2/3)^{1/2}$. The asymmetry parameter η takes values between 0 and 1, and P_Q becomes equal to C_Q when $\eta = 0$.

In the case of $I = 9/2$ as ^{93}Nb, P_Q values are obtained by

$$P_Q = \left(1224 \cdot \frac{10}{27}(\delta_{F1} - \delta_{F2})\right)^{1/2} \nu_L \cdot 10^{-3}. \quad (3)$$

RESULTS AND DISCUSSION

^{93}Nb NMR. Figures 2a and 2b show, respectively, the ^{93}Nb MAS NMR measurements using the spin-echo method[28] and 3QMAS NMR spectrum[29] for a powder sample of $Ba_3MoNbO_{8.5}$ at room temperature. In Figure 2a, two chemical shifts are observed at approximately −750 and −950 ppm, apart from the ghost signal called the spinning sideband. In general, MQMAS measurements are less sensitive than single-pulse MAS measurements, but as shown in Figure 2b, an adequate spectrum was obtained, and the distribution along the chemical shift axis is clearly shown for the more intense signal. From the peak position (δ_{F1}, δ_{F2}) in the contour map of the 3QMAS spectrum, the values of δ_{iso} and P_Q were estimated using Eqs. (1)–(3), and the results are listed in Table 2.

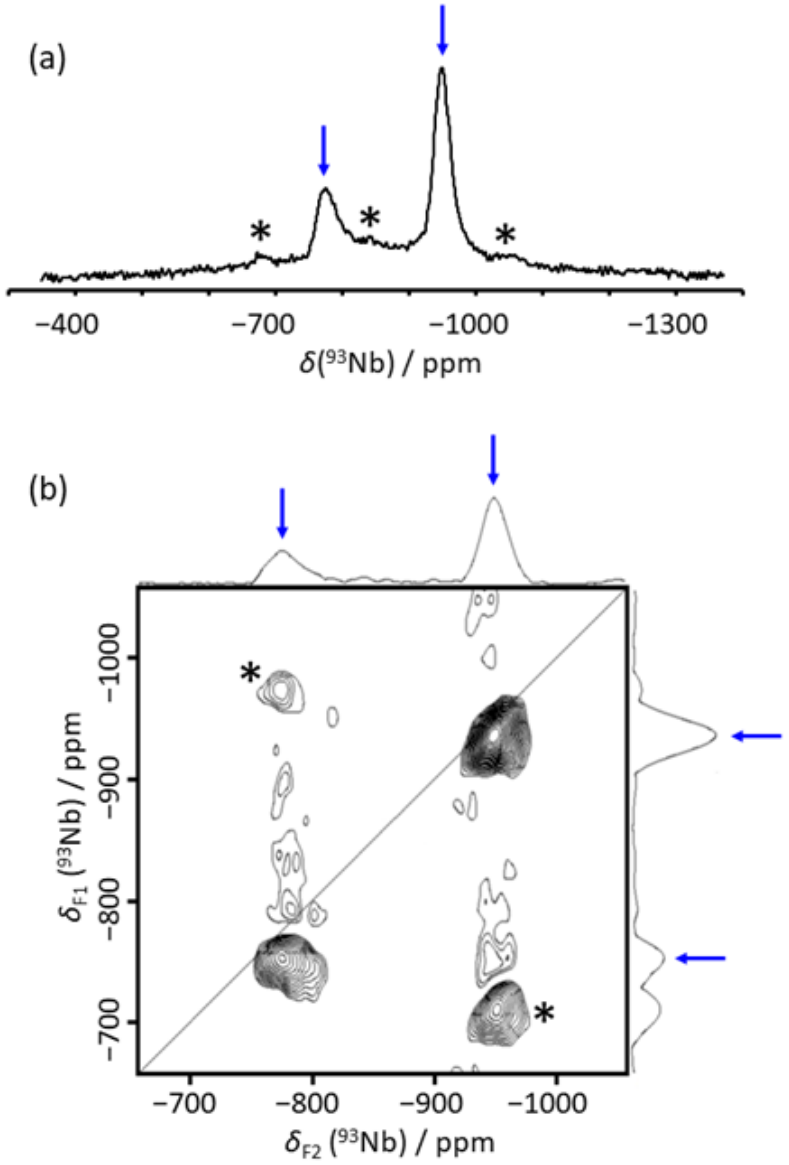

Figure 2. (a) ^{93}Nb MAS NMR and (b) ^{93}Nb 3QMAS NMR spectra of $Ba_3MoNbO_{8.5}$. The diagonal line in the 2D diagram is called the chemical shift axis; a spreading of the signal along the diagonal line indicates a distribution in chemical shift. Asterisks (*) denote spinning sidebands. Arrows indicate the position of each peak.

Table 2. δ_{F1}, δ_{F2}, δ_{iso}, and P_Q values obtained from ^{93}Nb 3QMAS measurements on $Ba_3MoNbO_{8.5}$, with attributed sites and attributed coordination numbers

δ_{F1} / ppm	δ_{F2} / ppm	δ_{iso} / ppm	P_Q / MHz	Attributed sites [a]	Attributed coordination number
−753	−775	−761	20	M1	4 (M1)
				(or M2)	(or 6 (M2))
−937	−949	−941	14	M1	6

[a]Both M1 and M2 are for (Nb/Mo) sites, and the notation is the same as in ref 7.

The more intense signal of −937 ppm is attributed to the following: the M1 and M2 sites are 88.1% and 11.9% of the total M sites, respectively.[14] Even with all Mo biased toward the M1 site notwithstanding,[20] Nb is 38.1% and 11.9% at the M1 and M2 sites, respectively. For the half-integer quadrupolar nuclei, the signal intensity ratio does not often reflect the quantity ratio due to the amplitude of the quadrupole coupling. However, as there is no significant difference in the P_Q values of the two peaks (Table 2), the ratio rather reflects the quantity ratio even in the echo measurement. Therefore, the signal at the M2 site in the non-conducting layer cannot be the strongest, so the more intense peak at −937 ppm is identified as the M1 site in the conducting layer. We considered three possible M1 site assignments: $M1O_4$, $M1O_5$, and $M1O_6$. The $M1O_5$ polyhedra has an intrinsically large P_Q value owing to its low symmetry, but its P_Q value of 14 MHz is much smaller than the value of a possible NbO_5 polyhedron of approximately 80 MHz; hence, the $M1O_5$ structure is excluded from consideration.[21,22] Of the $M1O_4$ and $M1O_6$ polyhedra, the P_Q values of NbO_6 and NbO_4 are reported to be 0–50 MHz and approximately 80 MHz, respectively, with NbO_6 tending to be smaller.[21,22] Moreover, in most niobium oxide

compounds, sites with higher coordination numbers tend to have more negative chemical shifts.[21–23] For example, in $Ba_4Nb_2O_9$, it has been reported that the δ_{iso} of NbO_4, NbO_5, and NbO_6 are −714 and −722 ppm; −822 and −871 ppm; and −818, −832, −865, and −931 ppm, respectively.[23] Therefore, of the two possibilities for the $M1O_4$ and $M1O_6$ polyhedra, the −937 ppm of δ_{iso} is attributed to the signal from the $Nb1O_6$ octahedron. In addition, the signal spread in the direction of the chemical shift axis in the 2D map is considered to be due to the M1 site being located within the conducting layer with a mixture of different local Mo/Nb structures.

For the less intense signal at −753 ppm of δ_{iso}, the evidence supporting attribution to $M1O_4$ and $M2O_6$ polyhedra is considerable. The $M1O_5$ polyhedron, however, cannot have a P_Q value as small as 20 MHz. For $M1O_4$, the relatively small P_Q value can be explained by the possibility that either the electric field gradient around the nucleus is averaged to some extent owing to thermal motions such as lattice vibrations, or the local structure is essentially symmetrical. $M2O_6$ was shifted exceptionally in the positive direction, compared to what is typically observed for NbO_6 octahedra.[21–23] Therefore, the signal is more likely due to $M1O_4$.

For the $M1O_5$ polyhedron, the lack of a 3QMAS signal suggests that either there are few $Nb1O_5$ polyhedra or the line broadening due to large quadrupolar interactions prevented them from being observed.[22] Here, in reference 23, a case with the small C_Q values is reported for 5-coordinated structures, but we believe that these values should not be used as a reference for the following two reasons. The first reason is the exceptionally small C_Q values for similar line widths in this literature compared to our data and other literature. As shown in Equation (2), different P_Q or C_Q values are obtained for the same line width depending on the magnitude of I. This may be because the formula for $I = 3/2$, which is used in many nuclei, was incorrectly used

in the analysis for ^{93}Nb, where $I = 9/2$. The second reason is that the 5-coordination studied in $Ba_3MoNbO_{8.5}$ does not depend on hydration, and the 5-coordination by hydration as described in the literature may cause line width sharpening due to accelerated molecular motion.

^{95}Mo NMR. Figures 3a, b, and c show the results of ^{95}Mo MAS NMR measurements of the powder samples of $Ba_3MoNbO_{8.5}$ at room temperature by the single pulse method, ^{95}Mo-enriched $Ba_3MoNbO_{8.5}$ by the single pulse method, and ^{95}Mo-enriched $Ba_3MoNbO_{8.5}$ by the spin-echo method,[28] respectively. In Figure 3a, two signals were observed at approximately −40 ppm to −50 ppm. One is a sharp doublet-like signal typical of half-integer spin quadrupole nuclei in axially-symmetric sites observed at approximately −40 ppm with $\eta \sim 0$, as simulated in Figure 3d,[30] and the other is a broad signal with a clear tail to low frequency at approximately −50 ppm. The C_Q and δ_{iso} values obtained from the DMFIT simulation software for the narrow peak at approximately −40 ppm (Figure 3b) and the peak position of the broad signal are listed in Table 3. According to published reports, the ^{95}Mo chemical shifts of the MoO_4 tetrahedron in salts cover a wide range of values, from 131 ppm in $CdMoO_4$ to −122 ppm in $CsLiMoO_4$.[24,25] The ^{95}Mo chemical shifts of the MoO_6 octahedron in salts range from 205 to 29 ppm for three sites of $[(NH_4)_6Mo_7O_{24}]\cdot 4H_2O$.[26] Therefore, it is difficult to discuss the coordination number only in terms of the magnitude of the shift. Notably, the C_Q values of ^{95}Mo are less than those of ^{93}Nb because those values are dependent on the properties of each nucleus. The signal at −40 ppm has a C_Q of 1.8 MHz, within the normal tetrahedral and octahedral values of 0–3 MHz;[24–26] hence, we can exclude $M1O_5$, which cannot have spherical symmetry and therefore should have a larger C_Q. Furthermore, $M1O_4$ is also excluded, as its asymmetry parameter cannot be zero because O3 oxygen does not have axial C_3 symmetry. The M2 site can be split into two equivalent sites,[14] but the M2 sites have axial C_3 symmetry; hence, it is reasonable to simulate

the signal with it when the asymmetry parameter is zero, as shown in Figure 3d. As for M1 site, it also may have axial C_3 symmetry when it only adopts the $M1O_6$ structure; hence, it is possible that this signal is derived from $M1O_6$. However, the M1 site is considered to be affected by structural disorder due to the mixing of different local Mo/Nb structures in the conducting layer, even in the $M1O_6$ structure, and the axial-symmetrical signal is attributed to the M2 site in the non-conducting layer. Meanwhile, the broad signal with the tail at approximately −50 ppm is considered suitable to be attributed to one of the M1 sites, regardless of the coordination number, $M1O_4$, $M1O_5$, or $M1O_6$ in the conducting layer (Table 3). Here, for this peak, the distribution of chemical shifts due to the structural disorder renders obtaining the reliable C_Q value by line shape analysis difficult.

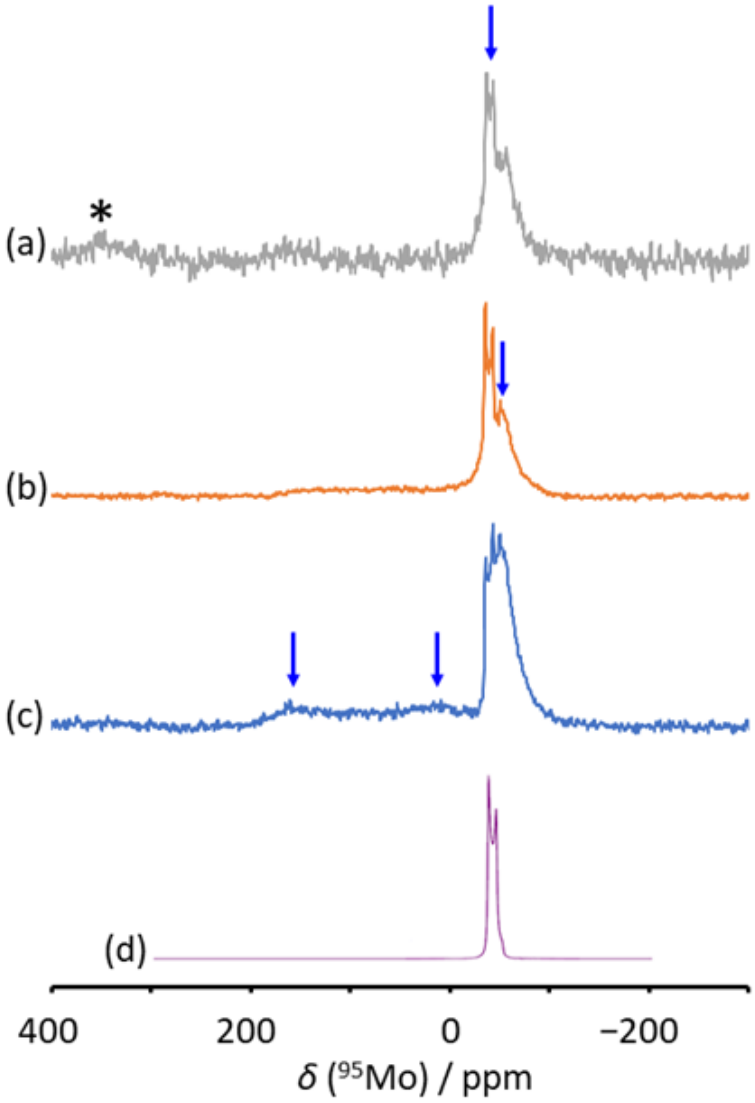

Figure 3. ^{95}Mo MAS NMR spectra of (a) $Ba_3MoNbO_{8.5}$ measured by the single pulse method, (b) ^{95}Mo-enriched $Ba_3NbMoO_{8.5}$ measured by the single pulse method, (c) ^{95}Mo-enriched $Ba_3MoNbO_{8.5}$ measured by the Oldfield echo method and (d) the DMFIT simulation[30] result for the sharp peak around −40 ppm. The asterisk (*) indicates a spinning sideband. Arrows indicate the position of each peak.

Table 3. ^{95}Mo peak positions, isotropic chemical shifts, quadrupolar parameters, attributed sites, and attributed coordination numbers for $Ba_3MoNbO_{8.5}$

δ_{MAS} / ppm	δ_{iso} / ppm	C_Q / MHz	η	Attributed sites [a]	Attributed coordination number
160	–	–	–	M1	4, 5, or 6
10	–	–	–	M1	4, 5, or 6
−50	–	–	–	M1	4, 5, or 6
	−33	1.8	0[b]	M2	6

[a]Both M1 and M2 are for (Nb/Mo) sites, and the notation is the same as in ref. 7.

[b]In the present simulation, this value was fixed at 0 for axial C_3 symmetry.

The peak at approximately +350 ppm in Figure 3a is a spinning sideband; however, another signal that appears at approximately +160 ppm has not been assigned. We will now discuss the possible assignment of this peak.

When we measured a sample enriched with ^{95}Mo, the signal-to-noise ratio was greatly improved, as shown in Figure 3b, but the width of the signal appears to increase between +200 ppm and 0 ppm. Because the single-pulse MAS measurements shown in Figures 3a and 3b tend to distort the baseline due to the phase shift, the echo method was used to measure the ^{95}Mo-enriched sample, and a signal was observed at +10 ppm, in addition to +160 ppm, as listed in Table 3. The echo method has the disadvantage of a low signal-to-noise ratio and a deviation between intensity and volume ratios related to the amplitude of the quadrupolar coupling; however, it is known for its low baseline distortion.

The two chemical shifts at +160 and +10 ppm in Figure 3c may originate from different sites or from a single site. If they originate from different sites, the chemical shift at approximately +10 ppm is related to a different local structure than the peak at +160 ppm, and it is reasonable to attribute each of the three peaks at +160, +10, and −50 ppm to one of the three polyhedra, $M1O_4$, $M1O_5$, or $M1O_6$ (Table 3). If both peaks originate from a single site, this implies that a broad spectrum ranging from +160 to +10 ppm has a C_Q of 8 MHz and η of almost 0 (refer to the Supporting Information). This C_Q value is much larger than the values up to approximately 3 MHz that are typical for other MoO_4 and MoO_6 polyhedra.[24–26] Furthermore, because the P_Q results of ^{93}Nb are smaller than usual, it is natural that the C_Q values of ^{95}Mo at the same site are also smaller than usual; further, a larger-than-normal C_Q of 8 MHz is not possible for either the MoO_4 or MoO_6 polyhedra. To the best of our knowledge, no ^{95}Mo NMR spectra of MoO_5 polyhedra have been reported. However, large C_Q values are only possible for MoO_5 polyhedra, which are relatively difficult to form in a highly symmetric structure. Here, it is possible that η may be close to zero only for structures with near-axial symmetry, such as a square pyramid or a triangular bipyramid.[14,17] In both cases, therefore, the experimental data are mostly likely explained as MoO_5 polyhedra in the conducting layer, although the attribution of the broad chemical shifts observed is still unclear (Table 3).

CONCLUSIONS

The initial analysis of $Ba_3MoNbO_{8.5}$, using Rietveld refinement, suggested that the conducting layer contains only $M1O_4$ and $M1O_6$ polyhedra, whereas single-crystal analysis suggested the possibility of the presence of $M1O_5$ polyhedra. The presence of a five-coordinate $(Mo/Nb)O_5$ has

been suggested by reverse Monte-Carlo total neutron scattering; however, the results were not highly reliable. In this study, the local structure of $Ba_3MoNbO_{8.5}$ was investigated by individual ^{93}Nb and ^{95}Mo solid-state NMR measurements, which directly reflect the electronic state around $^{95}Mo/^{93}Nb$ nuclei. ^{93}Nb NMR data showed the presence of $Nb1O_6$ octahedra and either $Nb1O_4$ tetrahedra or $Nb2O_6$ octahedra. The NMR spectra of ^{95}Mo-enriched $Ba_3MoNbO_{8.5}$ showed four peaks; one was attributed to MoO_6 octahedra in the non-conducting layer, and the other three peaks could not be attributed, assuming there are only MoO_4 and MoO_6 polyhedra in the conducting layer. Therefore, it is concluded that a significant proportion of $Mo1O_5$ polyhedra is present in the oxide-ion conducting layer, and that Mo^{6+} plays a significant role in the enhanced conductivity of $Ba_3MoNbO_{8.5}$. The direct observation of the local structure by solid-state NMR is important for understanding the nature of ionic conduction and is an important tool in the development of solid electrolytes such as hexagonal perovskite-related oxide-ion conductors.

ASSOCIATED CONTENT

Supporting Information.

Results of the DMFIT simulation in the event that both the +160 and +10 ppm chemical shifts appear from the same local structure in the ^{95}Mo MAS NMR spectrum of ^{95}Mo-enriched $Ba_3MoNbO_{8.5}$ in Figure 3c (blue line). (PDF)

AUTHOR INFORMATION

Corresponding Author

*TANSHO.Masataka@nims.go.jp

Present Addresses$^{\nabla}$Department of Electronic Engineering, Graduate School of Engineering, Tohoku University, Sendai 987-8579, Japan.

Author Contributions

The manuscript was written through contributions of all authors. All authors have given approval to the final version of the manuscript.

Funding Sources

Any funds used to support the research of the manuscript should be placed here (per journal style).

Notes

The authors declare no competing financial interest.

ACKNOWLEDGMENTS

A part of this work was supported by NIMS microstructural characterization platform as a program of "Nanotechnology Platform" of the Ministry of Education, Culture, Sports, Science and Technology (MEXT), Japan, Grant Number JPMXP09A19NM0110. We express our gratitude to Dr. T. Shimizu and Mr. K. Deguchi of NIMS for their help with NMR measurements. We also express our gratitude to Mr. Y. Shimoikeda of Jeol Resonance Inc. for his help with MQMAS analysis.

ABBREVIATIONS

NMR, nuclear magnetic resonance; SOFCs, solid oxide fuel cells; MAS, magic angle spinning; MQ, multi-quantum; 3Q, three-quantum; SOQE, second-order quadrupolar effect.

REFERENCES

(1) Skinner, S. J. Recent Advances in Perovskite-Type Materials for Solid Oxide Fuel Cell Cathodes. *Int. J. Inorg. Mater.* **2001**, *3* (2), 113–121. https://doi.org/10.1016/S1466-6049(01)00004-6.

(2) Ishihara, T.; Matsuda, H.; Takita, Y. Doped LaGaO3 Perovskite Type Oxide as a New Oxide Ionic Conductor. *J. Am. Chem. Soc.* **1994**, *116* (9), 3801–3803. https://doi.org/10.1021/ja00088a016.

(3) Nakayama, S.; T., K.; Sadaoka, Y. Ionic Conductivity of Lanthanoid Silicates. $La_{10}(SiO_4)_6O_2$ (Ln = La, Nd, Sm, Gd, Dy, Y, Ho, Er and Yb). *J. Mater. Chem.* **1995**, *5* (5), 1801–1805.

(4) Lacorre, P.; Goutenoire, F.; Bohnke, O.; Retoux, R.; Lallgant, Y. Designing Fast Oxide-Ion Conductors Based on $La_2Mo_2O_9$. *Nature* **2000**, *404* (6780), 856–858. https://doi.org/10.1038/35009069.

(5) Li, M.; Pietrowski, M. J.; De Souza, R. A.; Zhang, H.; Reaney, I. M.; Cook, S. N.; Kilner, J. A.; Sinclair, D. C. A Family of Oxide Ion Conductors Based on the Ferroelectric Perovskite $Na_{0.5}Bi_{0.5}TiO_3$. *Nat. Mater.* **2014**, *13* (1), 31–35. https://doi.org/10.1038/nmat3782.

(6) García-González, E.; Parras, M.; González-Calbet, J. M. Electron Microscopy Study of a New Cation Deficient Perovskite-like Oxide: $Ba_3MoNbO_{8.5}$. *Chem. Mater.* **1998**, *10* (6), 1576–1581. https://doi.org/10.1021/cm9708022.

(7) Fop, S.; Skakle, J. M. S.; McLaughlin, A. C.; Connor, P. A.; Irvine, J. T. S.; Smith, R. I.; Wildman, E. J. Oxide Ion Conductivity in the Hexagonal Perovskite Derivative $Ba_3MoNbO_{8.5}$. *J. Am. Chem. Soc.* **2016**, *138* (51), 16764–16769. https://doi.org/10.1021/jacs.6b10730.

(8) Coduri, M.; Bernasconi, A.; Fischer, H. E.; Malavasi, L. The $Ba_3Mo_{1-x}W_xNbO_{8.5}$ ion Conductors: Insights into Local Coordination from X-Ray and Neutron Total Scattering. *J. Mater. Chem. A* **2020**, *8* (40), 21227–21240. https://doi.org/10.1039/d0ta07073d.

(9) Auckett, J. E.; Gutmann, M. J.; Evans, I. R. Understanding the Correlation between Oxide Ion Mobility and Site Distributions in $Ba_3NbWO_{8.5}$. *Inorg. Chem.* **2020**, *59* (19), 14245–14250. https://doi.org/10.1021/acs.inorgchem.0c02035.

(10) Fop, S.; Wildman, E. J.; Irvine, J. T. S.; Connor, P. A.; Skakle, J. M. S.; Ritter, C.; McLaughlin, A. C. Investigation of the Relationship between the Structure and Conductivity of the Novel Oxide Ionic Conductor $Ba_3MoNbO_{8.5}$. *Chem. Mater.* **2017**, *29* (9), 4146–4152. https://doi.org/10.1021/acs.chemmater.7b01298.

(11) Fop, S.; Wildman, E. J.; Skakle, J. M. S.; Ritter, C.; McLaughlin, A. C. Electrical and Structural Characterization of $Ba_3Mo_{1-x}Nb_{1+x}O_{8.5-x/2}$: The Relationship between Mixed Coordination, Polyhedral Distortion and the Ionic Conductivity of $Ba_3MoNbO_{8.5}$. *Inorg. Chem.* **2017**, *56* (17), 10505–10512. https://doi.org/10.1021/acs.inorgchem.7b01488.

(12) Yasui, Y.; Tsujiguchi, T.; Sakuda, Y.; Hester, J. R.; Yashima, M. Oxide-Ion Occupational Disorder, Diffusion Path, and Conductivity in Hexagonal Perovskite Derivatives $Ba_3WNbO_{8.5}$ and $Ba_3MoNbO_{8.5}$. *J. Phys. Chem. C* **2022**, *126* (5), 2383– 2393. https://pubs.acs.org/doi/10.1021/acs.jpcc.1c09416...

(13) Bernasconi, A.; Tealdi, C.; Malavasi, L. High-Temperature Structural Evolution in the $Ba_3Mo_{(1-x)}W_xNbO_{8.5}$ System and Correlation with Ionic Transport Properties. *Inorg. Chem.* **2018**, *57* (11), 6746–6752. https://doi.org/10.1021/acs.inorgchem.8b01093.

(14) Auckett, J. E.; Milton, K. L.; Evans, I. R. Cation Distributions and Anion Disorder in $Ba_3NbMO_{8.5}$ (M = Mo, W) Materials: Implications for Oxide Ion Conductivity. *Chem. Mater.* **2019**, *31* (5), 1715–1719. https://doi.org/10.1021/acs.chemmater.8b05179.

(15) Yashima, M.; Tsujiguchi, T.; Fujii, K.; Niwa, E.; Nishioka, S.; Hester, J. R.; Maeda, K. Direct Evidence for Two-Dimensional Oxide-Ion Diffusion in the Hexagonal Perovskite-Related Oxide $Ba_3MoNbO_{8.5-\delta}$. *J. Mater. Chem. A* **2019**, *7* (23), 13910–13916. https://doi.org/10.1039/c9ta03588e.

(16) Chambers, M. S.; Mccombie, K. S.; Auckett, J. E.; Mclaughlin, A. C.; Irvine, J. T. S.; Chater, P. A.; Evans, J. S. O.; Evans, I. R. Hexagonal Perovskite Related Oxide Ion Conductor $Ba_3NbMoO_{8.5}$: Phase Transition, Temperature Evolution of the Local Structure and Properties. *J. Mater. Chem. A* **2019**, *7* (44), 25503–25510. https://doi.org/10.1039/c9ta08378b.

(17) Fop, S.; McCombie, K.; Smith, R. I.; McLaughlin, A. C. Enhanced Oxygen Ion Conductivity and Mechanistic Understanding in $Ba_3Nb_{1-x}V_xMoO8.5$. *Chem. Mater.* **2020**, *32* (11), 4724–4733. https://doi.org/10.1021/acs.chemmater.0c01322.

(18) Fop, S.; McCombie, K. S.; Wildman, E. J.; Skakle, J. M. S.; Irvine, J. T. S.; Connor, P. A.; Savaniu, C.; Ritter, C.; Mclaughlin, A. C. High Oxide Ion and Proton Conductivity in a Disordered Hexagonal Perovskite. *Nat. Mater.* **2020**, *19* (7), 752–757. https://doi.org/10.1038/s41563-020-0629-4.

(19) Yashima, M.; Tsujiguchi, T.; Sakuda, Y.; Yasui, Y.; Zhou, Y.; Fujii, K.; Torii, S.; Kamiyama, T.; Skinner, S. J. High Oxide-Ion Conductivity through the Interstitial Oxygen Site in $Ba_7Nb_4MoO_{20}$-Based Hexagonal Perovskite Related Oxides. *Nat. Commun.* **2021**, *12* (1), 556. https://doi.org/10.1038/s41467-020-20859-w.

(20) Murakami, T.; Shibata, T.; Yasui, Y.; Fujii, K.; Hester, J. R.; Yashima, M. High Oxide-Ion Conductivity in a Hexagonal Perovskite-Related Oxide $Ba_7Ta_{3.7}Mo_{1.3}O_{20.15}$ with Cation Site Preference and Interstitial Oxide Ions. *Small* **2021**, *2106785*, 2106785. https://doi.org/10.1002/smll.202106785.

(21) Hanna, J. V.; Pike, K. J.; Charpentier, T.; Kemp, T. F.; Smith, M. E.; Lucier, B. E. G.; Schurko, R. W.; Cahill, L. S. A ^{93}Nb Solid-State NMR and Density Functional Theory Study of Four- and Six-Coordinate Niobate Systems. *Chem. - A Eur. J.* **2010**, *16* (10), 3222–3239. https://doi.org/10.1002/chem.200901581.

(22) Papulovskiy, E.; Shubin, A. A.; Terskikh, V. V.; Pickard, C. J.; Lapina, O. B. Theoretical and Experimental Insights into Applicability of Solid-State ^{93}Nb NMR in Catalysis. *Phys. Chem. Chem. Phys.* **2013**, *15* (14), 5115–5131. https://doi.org/10.1039/c3cp44016h.

(23) Dunstan, M. T.; Blanc, F.; Avdeev, M.; McIntyre, G. J.; Grey, C. P.; Ling, C. D. Long-Range-Ordered Coexistence of 4-, 5-, and 6-Coordinate Niobium in the Mixed Ionic-Electronic Conductor γ-$Ba_4Nb_2O_9$. *Chem. Mater.* **2013**, *25* (15), 3154–3161. https://doi.org/10.1021/cm4014656.

(24) Mastikhin, V. M.; Lapina, O. B.; Maximovskaya, R. I. ^{95}Mo Solid-State NMR Spectra of Molybdates. *Chem. Physic Lett.* **1988**, *148* (5), 413–416.

(25) Forgeron, M. A. M.; Wasylishen, R. E. Molybdenum Magnetic Shielding and Quadrupolar Tensors for a Series of Molybdate Salts: A Solid-State ^{95}Mo NMR Study. *Phys. Chem. Chem. Phys.* **2008**, *10* (4), 574–581. https://doi.org/10.1039/b713276j.

(26) De Lacaillerie, J. B. D. E.; Barberon, F.; Romanenko, K. V.; Lapina, O. B.; Pollès, L. Le; Gautier, R.; Gan, Z. ^{95}Mo Magic Angle Spinning NMR at High Field: Improved Measurements and Structural Analysis of the Quadrupole Interaction in Monomolybdates and Isopolymolybdates. *J. Phys. Chem. B* **2005**, *109* (29), 14033–14042. https://doi.org/10.1021/jp0519621.

(27) Johnston, K. E.; Griffin, J. M.; Walton, R. I.; Dawson, D. M.; Lightfoot, P.; Ashbrook, S. E. ^{93}Nb NMR and DFT Investigation of the Polymorphs of $NaNbO_3$. *Phys. Chem. Chem. Phys.* **2011**, *13* (16), 7565–7576. https://doi.org/10.1039/c1cp20258h.

(28) Kunwar, A. C.; Turner, G. L.; Oldfield, E. Solid-State Spin-Echo Fourier Transform NMR of ^{39}K and ^{67}Zn Salts at High Field. *J. Magn. Reson.* **1986**, *69* (1), 124–127. https://doi.org/10.1016/0022-2364(86)90224-6.

(29) Amoureux, J. P.; Fernandez, C.; Steuernagel, S. Z Filtering in MQMAS NMR. *Journal of Magnetic Resonance - Series A*. **1996**, *123* (1), 116–118. https://doi.org/10.1006/jmra.1996.0221.

(30) Massiot, D.; Fayon, F.; Capron, M.; King, I.; Le Calvé, S.; Alonso, B.; Durand, J. O.; Bujoli, B.; Gan, Z.; Hoatson, G. Modelling One- and Two-Dimensional Solid-State NMR Spectra. *Magn. Reson. Chem.* **2002**, *40* (1), 70–76. https://doi.org/10.1002/mrc.984.

(31) Iijima, T.; Kato, S.; Ikeda, R.; Ohki, S.; Kido, G.; Tansho, M.; Shimizu, T. Structure of Duplex Oxide Layer in Porous Alumina Studied by ^{27}Al MAS and MQMAS NMR. *Chem. Lett.* **2005**, *34* (9), 1286–1287. https://doi.org/10.1246/cl.2005.1286.

(32) Engelhardt, G.; Kentgens, A. P. M.; Koller, H.; Samoson, A. Strategies for Extracting NMR Parameters from ^{23}Na MAS, DOR and MQMAS Spectra. A Case Study for $Na_4P_2O_7$. *Solid State Nucl. Magn. Reson.* **1999**, *15* (3), 171–180. https://doi.org/10.1016/S0926-2040(99)00054-5.

(33) Amoureux, J. P.; Fernandez, C. Triple, Quintuple and Higher Order Multiple Quantum MAS NMR of Quadrupolar Nuclei. *Solid State Nucl. Magn. Reson.* **1998**, *10* (4), 211–223. https://doi.org/10.1016/S0926-2040(97)00027-1.

(34) Anupõld, T.; Reinhold, A.; Sarv, P.; Samoson, A. A Comparison of Double Rotation and Multi-Quantum Magic Angle Spinning Spectra. *Solid State Nucl. Magn. Reson.* **1998**, *13* (1–2), 87–91. https://doi.org/10.1016/S0926-2040(98)00068-X.

(35) Tansho, M.; Suehiro, T.; Shimizu, T. Constancy of the Quadrupolar Interaction Product in Nanocrystalline Gallium Nitride Revealed by ^{71}Ga MAS NMR Shift Distribution. *Solid State Nucl. Magn. Reson.* **2019**, *97*, 25–30. https://doi.org/10.1016/j.ssnmr.2018.08.006.

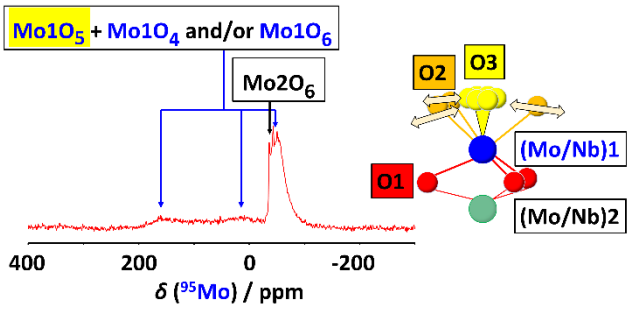

TOC Graphic